Biomechanics-Aware Trajectory Optimization for Navigation during Robotic Physiotherapy

Italo Belli 1.2*, J. Micah Prendergast 1, Ajay Seth 2, and Luka Peternel 1.

Abstract-Robotic devices hold promise for aiding patients in orthopedic rehabilitation. However, current robotic-assisted physiotherapy methods struggle including biomechanical metrics in their control algorithms, crucial for safe and effective therapy. This paper introduces BATON, a Biomechanics-Aware Trajectory Optimization approach to robotic Navigation of human musculoskeletal loads. The method integrates a highfidelity musculoskeletal model of the human shoulder into realtime control of robot-patient interaction during rotator cuff tendon rehabilitation. We extract skeletal dynamics and tendon loading information from an OpenSim shoulder model to solve an optimal control problem, generating strain-minimizing trajectories. Trajectories were realized on a healthy subject by an impedance-controlled robot while estimating the state of the subject's shoulder. Target poses were prescribed to design personalized rehabilitation across a wide range of shoulder motion avoiding high-strain areas. BATON was designed with real-time capabilities, enabling continuous trajectory replanning to address unforeseen variations in tendon strain, such as those from changing muscle activation of the subject.

Index Terms—Physical Human-Robot Interaction, Optimization and Optimal Control, Rehabilitation Robotics, Musculoskeletal Dynamics, OpenSim.

I. INTRODUCTION

NJURIES affecting the musculoskeletal system are pervasive in society due to increasing population longevity, strenuous manual labor, and greater engagement in sports [1]-[3]. At the forefront of these injuries, disorders impacting the shoulder and the rotator cuff are particularly common, with clinical literature reporting their prevalence to be as high as 22% in the general population [1]. Overall, the demand for therapy and rehabilitation is large and expected to grow, exacerbating the problem posed by a lack of physical therapists. Moreover, the task of treating a complex biological mechanism, such as the shoulder, is challenging due to a fundamental lack of insights into rotator-cuff behavior. Physiotherapists need to move the joint safely, gradually increasing the patient's range of motion while physically supporting the patient's arm and avoiding re-injuries [4]. Consequently, simple and limited movements are prescribed, to limit both the risk of re-injury and the physical demands on the therapist to manually manipulate the patient safely.

Robotic technologies can assist in addressing these two gaps during therapy: robots can reduce the manual burden on physiotherapists and provide new tools to monitor and

The authors are with the ¹Cognitive Robotics and the ²BioMechanical Engineering departments, Delft University of Technology, Delft, The Netherlands (email: i.belli@tudelft.nl, j.m.prendergast@tudelft.nl, a.seth@tudelft.nl, l.peternel@tudelft.nl)

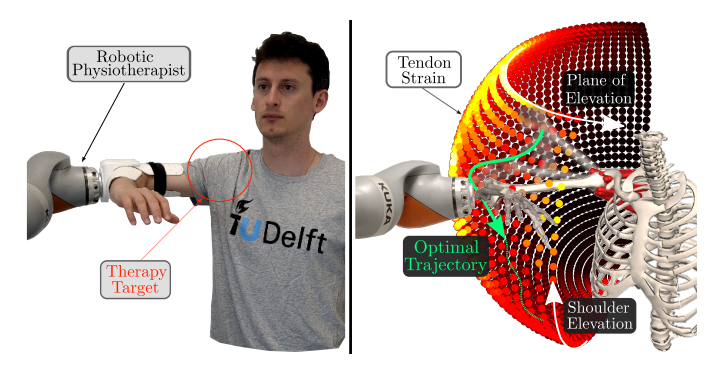


Fig. 1. BATON combines musculoskeletal modeling and human-robot interaction to enable a robotic physiotherapist to plan therapeutic movements for its patients in real-time while considering tissue loading (i.e. strain) induced in the rotator cuff tendons in the shoulder.

improve rehabilitation outcomes. Overall, rehabilitative robots are already used successfully in post-stroke rehabilitation [5]-[7] and gait assistance [8]–[10]. However, robots to treat musculoskeletal injuries (such as rotator cuff tears) remain limited. In particular, previous work remains focused on relieving physiotherapists from physically manipulating the patient. Smooth rehabilitation trajectories can be guaranteed by focusing on the control of the movement of the rehabilitative robot itself [11], and therapeutic robotic movements can be learned from expert human demonstrations to automate manual patient manipulation [12]. However, these solutions do not directly account for the patient's biomechanics. Deeper insights into human musculoskeletal mechanics can enable robots to be aware of tissue and joint loads associated with injury risks, allowing them to operate autonomously or in collaboration with therapists to holistically improve the rehabilitation process [13]. An increasingly promising strategy is to leverage human musculoskeletal models and incorporate them directly into robot control loops [14]-[19].

Musculoskeletal modeling has progressed greatly over the past decades, allowing researchers to estimate the activities of individual muscles involved in producing movement [20]–[22] and to perform predictive simulations of human motion [23], [24]. As computational models increasingly capture the inner workings of the human body, their applicability continues to expand, particularly in physical human-robot interaction and assistive devices. Recently, biomechanical models have been used to quantify assistance needed by a human operator [14]–[16], reduce human metabolic cost in walking-assistive devices [17]–[19], and even plan search-and-rescue robotic operations [25] or the motion of supernumerary robotics limbs [26]. Through computer simulations or offline usage

^{*}Corresponding Author: Italo Belli

of human models, these works demonstrated the importance and utility of including human biomechanics in robot planning and decision-making. However, they did not leverage highfidelity biomechanical simulations to regulate human-robot interactions in scenarios that require online adaptation to human behavior.

When real-time capabilities are necessary, purely kinematic models have been used to monitor human joint positions, velocities, and torques [27], or to develop controllers for hybrid neuroprostheses of the knee [28]. While lower-fidelity models allow for computational efficiency, they are unsuitable for insights into the musculoskeletal system during shoulder rehabilitation. Biomechanical quantities from a high-fidelity human model were recently used in an online model predictive control framework, achieving predictive control of a leg prosthesis for ergonomically safe walking [29]. Fast predictions of the user's knee torque were achieved through Bayesian interaction primitives, which could estimate the unobservable biomechanical values via the inclusion of a musculoskeletal model in the data augmentation offline. However, this study did not consider the mechanical behavior of the human tissues (e.g., muscles and tendons).

Building on the previously discussed applications of musculoskeletal models, we can go further to gain insights into the underlying biological tissues that are targets of physical therapy. By estimating tissue loads from external measurements based on a high-fidelity model of the human shoulder, we introduced the concept of "strain maps" [30] to capture the relationship between human pose and the strain (i.e., load) induced in the rotator cuff tendons. Abstracting the rotator cuff tendon strains into an intuitive and navigable map, we achieved offline graph-based motion planning for safe robotic-mediated shoulder rehabilitation [30]. However, the planning algorithm did not account for the dynamics of the human, resulting in trajectories that presented sudden direction changes and were potentially difficult to track. Accelerations imposed on the human shoulder were not monitored, and the trajectories were executed in an open loop. Employing the strain maps, we implemented a reactive impedance-control-based approach to physical human-robot interaction in rehabilitation that enabled a subject to perform therapeutic exercises while robotic assistance protected them from potentially dangerous poses [31]. The system would react only when dangerous movements were already initiated, without anticipating the subject's trajectory to prevent abrupt movements and experience high corrective forces from the robot.

Other researchers designed optimized trajectories for controlling an ankle rehabilitation robot, to minimize joint loading [32]. A custom ankle model was used to plan the robot's trajectory offline, making online adjustments based on tracking errors attributed to excessive joint stiffness. However, the human model was not considered during the adjustments, so the reference path could become suboptimal during execution.

To the best of our knowledge, a high-fidelity model of the human musculoskeletal system has never been used to synthesize adaptive robotic rehabilitative movements in real-time through coupled predictive simulations of human dynamics and tissue loading. Our primary objective is to develop a Biomechanics-Aware Trajectory Optimization for the Navigation of human tissue strains during robotic physiotherapy (BATON). Our novel approach intends to directly couple a state-of-the-art biomechanical model of the human shoulder to robotic control, generating movements for predictive robotic-assisted rotator cuff tendon rehabilitation in real-time. The resulting optimized trajectories are realized by a collaborative robot arm that delivers the movement to a healthy human subject through safe impedance control, with gravity compensation for the human arm naturally and adaptively provided by the model. This allows personalized treatment in the early stages of post-traumatic rehabilitation of the rotator cuff, where the subject does not support the weight of their own arm.

Our specific aims and contributions are:

- develop an automated system (BATON) to navigate underlying human biomechanical outcomes in real-time during robotic-assisted physiotherapy;
- design of an optimal control problem (OCP) for trajectory optimization that incorporates a real-time shoulder musculoskeletal model by decoupling skeletal dynamics and strain behavior;
- analyse performance both in simulation and on a physical robotic system applied to a test subject to demonstrate 1) the effect of OCP parameters on the planned trajectory, 2) the quality of the executed paths, 3) the ability to re-plan online based on changing strain landscapes, 4) real-time computational performance.

An intuitive analogy for navigating around potentially unsafe movements in human rehabilitation is the path planning of an autonomous ship in a bay where underwater reefs are present. To know which maneuvers allow the ship to navigate safely and efficiently toward a target position, we need both a dynamic model of the vessel and a map of the underwater reefs, providing non-obvious insights about the safest path. In our situation, the human shoulder dynamics play the role of the vessel, while the strain maps offer insights into what happens beneath the surface (specifically in the recovering tendons). Only by considering the two elements jointly can safe navigation be obtained.

II. METHODS

Our approach joins high-fidelity human biomechanics, trajectory optimization, and robot control to generate safe rehabilitation trajectories based on real-time underlying biomechanical insights (Fig. 2). We present our method for extracting insights from the musculoskeletal model for real-time use in optimization and control in Section II-A. Low-strain rehabilitation movements are planned towards target human poses by solving a trajectory optimization problem, detailed in Section II-B. A collaborative KUKA LBR iiwa 7 robotic arm is employed to estimate the current human pose (Section II-D) and to deliver the actual rehabilitation movement to the human subject during therapy. Details about the robot's control are given in Section II-E, and our experimental design is presented in Section II-F.

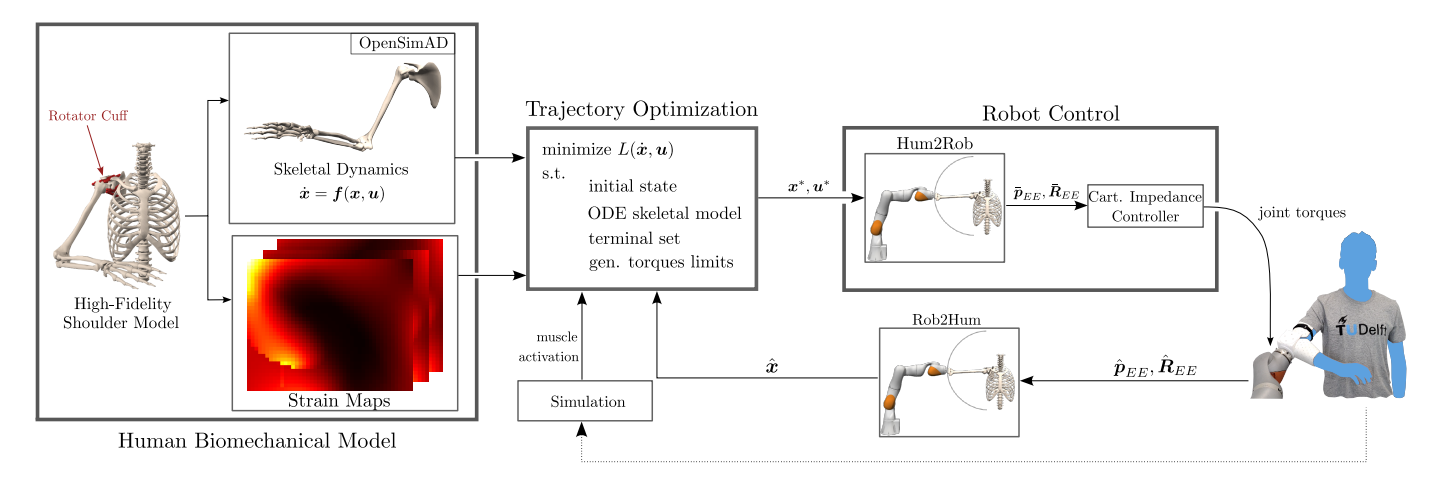


Fig. 2. Methodological overview of BATON applied to shoulder physiotherapy. The high-fidelity biomechanical model of the human shoulder (left) is split into skeletal dynamics and rotator cuff tendon loading information (strain maps). An optimal control problem computes safe rehabilitation movements leveraging insights from the human model, and its output is transformed into equivalent references for the robotic controllers to track. The robot's feedback is used to close the sensing loop on the current human status.

A. Human Biomechanical Model

We employ a high-fidelity biomechanical model of the human shoulder [33] to capture the human response in a computer simulation and predict how movements and forces will affect the tendons' strain in the rotator cuff. The human model, developed in OpenSim [34], [35], captures the shoulder's movement degrees of freedom (DoFs) and the muscles powering it. As such, it can inform the robot's controller of the internal tissue and skeletal mechanics during the physical human-robot interaction. In particular, we are interested in measures related to injury risk of the rotator cuff muscles (i.e., supraspinatus, subscapularis, infraspinatus, and teres minor), which act as stabilizers for the glenohumeral joint in the shoulder and whose tendons are subject to tears due to overuse. Mechanical strain is associated with re-injury risk of rotator cuff tendons, as excessive stretching of a healing tendon could lead to damages [36].

In the human body, the rotator cuff spans the glenohumeral joint, which permits mobility of the upper arm (humerus) with respect to the shoulder blade (scapula) through 3 DoFs. As such, we extracted a reduced-order model of the human shoulder, capturing the mobility of this joint alone (see Fig. 2, left). The state of the resulting human model is described as:

$$\boldsymbol{x} = [PE, \dot{PE}, SE, \dot{SE}, AR, \dot{AR}]^T \tag{1}$$

where PE, SE and AR are the 3 movement DoFs defined as the Y-X'-Y" sequence of intrinsic Euler angles in the fixed shoulder reference frame (PE: plane of elevation, SE: shoulder elevation as rotation around -X, AR: axial rotation, visualized in Fig. 3), and PE, SE and AR are their corresponding derivatives with respect to time. The arm size and mass of our human subject were used to personalize the model's properties through OpenSim's scaling functionalities and tabulated anthropometric data [37].

The personalized shoulder model specifies how the shoulder moves under the influence of applied torques/forces, and how these affect the underlying musculoskeletal system. However, embedding the model directly to plan rehabilitation movements through the OpenSim API is not computationally tractable for real-time applications. To achieve real-time performances without sacrificing model accuracy, we decouple tissue mechanics describing tendon strain changes with shoulder movement from skeletal dynamics that simulate how shoulder motion is generated as a consequence of applied forces. This decoupling enables us to retain the information contained in the original OpenSim model and access it much more rapidly, to formulate the problem of navigating shoulder motion over strain maps governed by skeletal dynamics.

1) Generating differentiable strain maps: the musculoskeletal model can be queried to provide quantitative information on the mechanical strain σ of a desired tendon in the rotator cuff. Biologically, the model's state x and the activation level $\alpha \in [0,1]$ of the corresponding muscle determine tendon strain, which can be expressed as:

$$\sigma = \frac{l_T(\boldsymbol{x}, \alpha) - l_0}{l_0} \cdot 100\%. \tag{2}$$

where $l_T(\boldsymbol{x}, \alpha)$ is the current length of the tendon and l_0 its slack length at rest. Querying the model for tendon strains during motion planning is impractical due to the computationally intensive calculations involved. Similar to our previous work, we can fully describe the change in strain σ based on the human model's state via pre-computed "strain maps" [30], [31], [38]. In the present work, we ignore the dependence on tendon velocity since rehabilitation movements are generally slow. With this assumption, we spanned the space of possible arm configurations and rotator cuff muscle activations to query the model for the tendon strain induced in every tendon of the rotator cuff. During this pre-computation phase, fixed 4degree steps were used to vary the movement DoFs within the shoulder range of motion, while muscle activation was varied at 0.005 discretization. In this way, we created highdimensional strain maps for every individual tendon, which allowed us to target only one tendon at a time or, alternatively, to monitor the strain on the rotator cuff as a whole by constructing aggregate maps that consider the highest strain across all the tendons [30], [38]. To simplify the understanding of strain level for non-expert users of our system (e.g., physiotherapists and patients), we chart σ on 2D grids where the strain percentage is visualized as a function of PE and SE angles, while both AR and the muscular activation α are fixed. To consider different values of AR and α , other (precomputed) 2D maps can be traversed.

As a final step, we interpolated our discrete strain maps using 2D Gaussian radial basis functions to leverage more efficient gradient-based methods in our trajectory optimization problem (Section II-B). Through least-squares fitting, we obtain the parameter vector $\boldsymbol{\pi} \in \mathbb{R}^{N_p \times N_G}$ that describes the combination of the N_G Gaussian functions best approximating every 2D strain map, in terms of the N_p parameters of every Gaussian.

2) Obtaining differentiable skeletal dynamics: after computing navigable differentiable maps of rotator cuff tendon strain, we need to account for the human movement dynamics governing how the human shoulder should be moved by the robot. This information can be obtained from the OpenSim model only numerically, and this has led researchers to employ less efficient gradient-free optimization methods to optimize human-robot interaction [26]. To enhance computational efficiency, we employed OpenSimAD [39] as a tool that allows us to retrieve a differentiable function from an OpenSim musculoskeletal model. OpenSimAD is an instrumented version of OpenSim recently developed to automatically generate the differentiable version of OpenSim outcomes and functions. It records the entire call sequence of the function used to compute a particular outcome variable of interest within the OpenSim model, offering the possibility to employ this call sequence for algorithmic differentiation by programs like CasADi [40]. In particular, we customized the OpenSimAD pipeline to obtain a differentiable representation of our reduced-order model of the human shoulder in terms of a set of ordinary differential equations that describe the dynamics of the state $oldsymbol{x} \in \mathbb{R}^{N_x}$ of the multibody skeletal system, given a set of generalized forces $oldsymbol{u} \in \mathbb{R}^{N_q}$ acting on the model's DoFs:

$$\dot{\boldsymbol{x}} = f(\boldsymbol{x}, \boldsymbol{u}),\tag{3}$$

where $N_q=3$ and $N_x=2N_q$ in our case. Importantly, this procedure guarantees that the model's joint definitions will be preserved, together with personalized dimensions, mass, and inertia for every existing bone in the original model.

B. Biomechanics-aware trajectory optimization

We combine information from the differentiable strain maps and human dynamics to formulate a biomechanics-aware optimal control problem (OCP), with the goal of synthesizing safe human motion towards a target shoulder position. The solution to the OCP is the optimal trajectory \boldsymbol{x}^* and corresponding generalized forces \boldsymbol{u}^* driving the human model toward the goal pose. The sequence of optimal controls and states $\{\boldsymbol{x}^*, \boldsymbol{u}^*\}$ is then transformed into a reference for the robot controller to deliver optimal rehabilitation motion to the human subject.

We opted to plan trajectories that are fully contained in a single 2D strain map, so that the output of our optimization would be intuitive for non-expert users and easy to visualize in two dimensions (e.g., on a computer screen). We selected plane of elevation (PE) and shoulder elevation (SE) to be our controlled DoFs, while current values of axial rotation (AR) and muscle activation α are input to select the strain map to plan onto.

We define below the key elements of the OCP (i.e., cost function and constraints) that allow us to set the optimality criterion with respect to which $\{x^*, u^*\}$ are found.

- 1) Cost Function: we design our cost function to capture important requirements for a safe rehabilitation trajectory: the movement should minimize the strain on selected tendons, produce low accelerations on the human body, and evolve towards the target final position. These elements are mirrored into the definition of our cost $L(\boldsymbol{x}(t), \dot{\boldsymbol{x}}(t))$, formalized as a weighted sum of the following terms:
 - $L_{\sigma} = \sigma(x, \alpha)$, accounting for the instantaneous (non-negative) strain that the selected tendon undergoes;
 - $L_{\rm acc} = \dot{\boldsymbol{x}}^T \boldsymbol{Q}_1 \dot{\boldsymbol{x}}$, accounting for the derivatives of our state variables during the motion. The positive semidefinite matrix $\boldsymbol{Q}_1 \in \mathbb{R}^{6 \times 6}$ allows us to consider only the relevant accelerations when planning on the current strain map;
 - $L_{\tau} = \frac{1}{d_0^2} (\boldsymbol{x} \boldsymbol{x}_{\tau})^T \boldsymbol{Q_2} (\boldsymbol{x} \boldsymbol{x}_{\tau})$, accounting for the distance to the target human model pose \boldsymbol{x}_{τ} , where d_0 represents the distance to the target pose at the beginning of the trajectory, to normalize the contribution of this term. Again, $\boldsymbol{Q_2} \in \mathbb{R}^{6 \times 6}$ is a positive semidefinite matrix selecting only the relevant human DoFs.

In the following, we will refer to the weights of these terms as w_{σ} , $w_{\rm acc}$ and w_{τ} respectively (where the latter does not include the normalization by d_0 introduced above).

- 2) Constraints: We apply constraints to ensure that the OCP solution can be executed safely on the human subject. Their definition and role is detailed below.
 - *Initial condition*: every new trajectory $\{x^*, u^*\}$ should start from the current state of the human model \hat{x}_{curr} , estimated through the robot's encoders (see Sec. II-D). The current state is used as the initial condition for the next instance of the OCP enforcing $x(t=0) = \hat{x}_{\text{curr}}$, where the initial time is set to be 0 without loss of generality.
 - *Torque limits*: to make sure that following the optimal trajectory does not require excessive torque to be exerted along the human DoF, we limit them within heuristic bounds by requiring $u_{\min} \leq u(t) \leq u_{\max}$, where $u_{\min}, u_{\max} \in \mathbb{R}^3$. Bounds can be adjusted to enforce different toque limits on the various DoF accounting, for example, for the fact that torques along SE should counteract gravity.
 - Terminal condition: to impose an acceptable final state for the human model, we prescribe that $(x_{t=T_f} x_\tau) \odot (x_{t=T_f} x_\tau) \le \epsilon$, where T_f represents the length of the planning horizon, and \odot the Hadamard product. If reaching the target final state is possible in the current OCP instance (e.g. if T_f is long enough), the parameter $\epsilon \in \mathbb{R}^6$ is defined for every element of the state vector, meaning both final pose and velocity of the human

model can be specified fully. Otherwise, if the target pose specified by x_{τ} is too far from \hat{x}_{curr} , only the final velocities are limited. This choice guarantees low velocities of the human arm at the end of the planning horizon and ensures recursive feasibility through a safe terminal set \mathbb{S}_T .

C. Optimal control problem (OCP) transcription

Overall, the optimal control problem that we aim to solve reads as follows:

$$\min_{\boldsymbol{x}(\cdot),\boldsymbol{u}(\cdot)} \int_0^{T_f} L\big(\boldsymbol{x}(t),\dot{\boldsymbol{x}}(t)\big) dt$$
 subject to:

$$egin{aligned} & m{x}(0) - \hat{m{x}}_{ ext{curr}} = m{0} & ext{initial state} \ & m{u}_{ ext{min}} \leq m{u}(t) \leq m{u}_{ ext{max}} & ext{torque limits} \ & m{x}_{t=T_f} \in \mathbb{S}_T & ext{terminal set} \end{aligned}$$

To solve the OCP, we cast it into discrete time, transcribing (4) into an equivalent Non-Linear Programming problem (NLP) that can be solved by structure-exploiting solvers. We achieved this with orthogonal collocation techniques [41], hence approximating the state trajectories with suitable dth-order polynomial splines. The overall optimization horizon T_f is broken down into N intervals of equal length, and inside the generic interval $[t_k, t_{k+1}]$ we select d=3 Legendre-Gauss collocation points at which the dynamics as in (3) are enforced. This step results in additional continuity and collocation constraints that need to be considered in the NLP formulation.

We implemented the resulting NLP in Python and solved it with IPOPT [42] leveraging MA27 [43] as a linear solver, while first- and second-order derivatives were provided by CasADi [40] and OpenSimAD. To clarify the computational advantage of using the differentiable skeletal dynamics, we also embedded numerically evaluated gradients with perturbation calls to the original OpenSim model directly in the collocation constraints of the NLP, through CasADi. We ran simulation experiments for both cases, to compare the computational requirements for both choices.

D. Human state estimation

The real-time trajectory optimization (4) formalized above requires the model's current state as input to initialize the next instance. We estimated the human model's pose on the basis of the position and orientation of the robot's end-effector (EE), which we mapped to the shoulder state \boldsymbol{x} according to the fixed rigid connection between the EE and elbow locked at 90° (see Fig. 3). An estimation of the full human pose is out of the scope of our current work, so we assume for simplicity that the center of the glenohumeral joint will be stationary during the experiments and that the orientation of the human torso is fixed. Under these conditions, monitored during the experiments, it is possible to reconstruct the shoulder state through the robot's encoders. Firstly, we observe that the

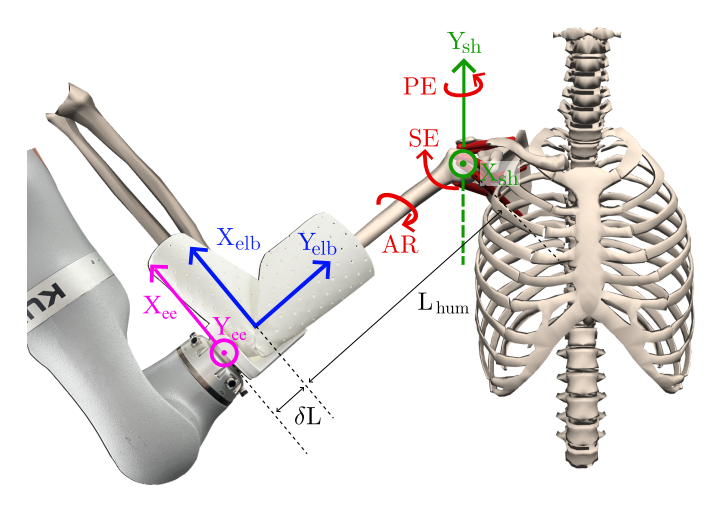


Fig. 3. Overview of the coordinate systems of the setup: The shoulder frame (green) originates in the center of the glenohumeral joint. The glenohumeral joint DoFs (PE, SE, and AR) are shown in red. The elbow frame (blue) originates in the center of the elbow, and a fixed transformation relates it to the robot's end-effector frame (pink).

orientation of the human elbow expressed in the reference frame of the human shoulder is 1:

$$^{\mathrm{sh}}\boldsymbol{R}_{\mathrm{elb}} = {^{\mathrm{sh}}\boldsymbol{R}_{\mathrm{base}}}^{\mathrm{base}}\hat{\boldsymbol{R}}_{\mathrm{EE}}(t)^{\mathrm{EE}}\boldsymbol{R}_{\mathrm{elb}},$$
 (5)

where *sh* denotes the shoulder frame, *base* the frame attached to the robot's base, and *elb* the frame fixed at the human elbow (see Fig. 3). The first and last rotations are known and fixed, while ${}^{\text{base}}\hat{R}_{\text{EE}}(t)$ can be estimated through the robot's forward kinematics. Moreover, following the definition of the glenohumeral DoFs in the human model [33], we can write:

$$^{\text{sh}}\mathbf{R}_{\text{elb}} = \mathbf{R}_y(PE)\mathbf{R}_x(-SE)\mathbf{R}_y(AR). \tag{6}$$

We first obtain our estimates \hat{PE} and \hat{SE} leveraging the end-effector position $\hat{p}_{EE}(t)$, and then estimate \hat{AR} through (6). Formally, we define a unit vector $\boldsymbol{\beta} \in \mathbb{R}^3$ expressing the direction of the humerus (upper arm) pointing from the center of the glenohumeral joint to the human elbow, and use its Cartesian components in the shoulder frame to estimate the human state:

$$\boldsymbol{\beta} = {}^{\text{sh}}\boldsymbol{R}_{\text{base}} \frac{{}^{\text{base}}\hat{\boldsymbol{p}}_{EE}(t) - {}^{\text{base}}\boldsymbol{p}_{\text{GH}}}{||{}^{\text{base}}\hat{\boldsymbol{p}}_{EE}(t) - {}^{\text{base}}\boldsymbol{p}_{\text{GH}}||_2^2}$$

$$\hat{PE} = \text{atan2}(\beta^x, \beta^z) \tag{7}$$

$$\hat{SE} = \arccos(\boldsymbol{\beta} \cdot [0 - 1 \ 0]^T)$$

where ${}^{\text{base}}p_{\text{GH}}$ is the known position of the center of the glenohumeral joint. Velocities of the generalized DoFs in the human model are estimated through the body twist of the last link of the robot, obtained through the robot's Jacobian:

$$^{ ext{base}}\hat{oldsymbol{
u}}_{ ext{EE}} = [^{ ext{base}}\hat{oldsymbol{
u}}_{ ext{EE}}^T \quad ^{ ext{base}}\hat{oldsymbol{
u}}_{ ext{EE}}^T]^T \in \mathbb{R}^6.$$
 (8)

Since the robot's EE and the human elbow are rigidly attached to each other, we can transform $^{base}\hat{\nu}_{EE}$ into the twist $^{sh}\hat{\nu}_{elb}$ through the known transformation:

$$^{\rm sh}\hat{\boldsymbol{\nu}}_{\rm elb} = \begin{bmatrix} \boldsymbol{R} & 0\\ 0 & \boldsymbol{R} \end{bmatrix}^{\rm base}\hat{\boldsymbol{\nu}}_{\rm EE} \tag{9}$$

¹we denote as ${}^Ip_k=[{}^Ip_k^x,{}^Ip_k^y,{}^Ip_k^z]^T\in\mathbb{R}^3$ the position of point k w.r.t. frame "I", and ${}^JR_{\rm I}\in SO(3)$ the rotation matrix to express it in frame "J".

where $R = {}^{\rm sh}R_{\rm elb}{}^{\rm elb}R_{\rm EE}{}^{\rm EE}R_{\rm base}$. Having retrieved \hat{PE} and \hat{SE} , ${}^{\rm sh}\hat{\nu}_{\rm elb}$ can be further transformed into ${}^{\rm sh'}\nu_{\rm elb}$, denoting the elbow twist expressed in the intermediate rotated frame where SE is defined (which we name sh'), and into ${}^{\rm sh''}\nu_{\rm elb}$, which denotes the elbow twist expressed in the frame where AR is defined (which we name sh''). Overall, we can obtain the velocity estimates for the human shoulder model as follows:

$$\hat{PE} = {}^{\text{sh}}\omega_{\text{elb}}^{y}, \quad \text{with} \quad {}^{\text{sh}}\omega_{\text{elb}} = \frac{{}^{\text{sh}}\boldsymbol{p}_{\text{elb}} \times {}^{\text{sh}}\boldsymbol{\hat{v}}_{\text{elb}}}{L_{\text{tot}}^{2}}$$

$$\hat{SE} = -{}^{\text{sh'}}\omega_{\text{elb}}^{x}, \quad \text{with} \quad {}^{\text{sh'}}\omega_{\text{elb}} = \frac{{}^{\text{sh'}}\boldsymbol{p}_{\text{elb}} \times {}^{\text{sh'}}\boldsymbol{\hat{v}}_{\text{elb}}}{L_{\text{tot}}^{2}} \quad (10)$$

$$\hat{AR} = {}^{\text{sh''}}\hat{\omega}_{\text{elb}}^{y}$$

where $L_{\rm tot} = L_{\rm hum} + \delta L$ is the distance between the center of the glenohumeral joint and the robot's EE (see Fig. 3), $^{\rm sh} \boldsymbol{p}_{\rm elb}$ is the position of the human elbow expressed in the shoulder frame, and $^{\rm sh'} \boldsymbol{p}_{\rm elb}$ is the equivalent quantity expressed in the sh' frame.

E. Robot control and model-based gravity compensation

Apart from being used for human pose estimation, the key purpose of the robotic arm is to deliver therapeutic motion to the human subject based on the continuously optimized trajectory. We map the optimal trajectory x^* resulting from (4) into the corresponding robot's end-effector reference pose:

$$^{\text{base}}\bar{\boldsymbol{R}}_{\text{EE}} = {}^{\text{base}}\boldsymbol{R}_{\text{sh}}{}^{\text{sh}}\boldsymbol{R}_{\text{elb}}(\boldsymbol{x}^*)^{\text{elb}}\boldsymbol{R}_{\text{EE}}$$
 (11)

$$base \bar{p}_{EE} = base p_{GH} + base \bar{R}_{EE}^{EE} p_{GH}$$
 (12)

Equations (11)-(12) ensure that the robot's end-effector pose is consistent with the desired trajectory for the human. Given the optimal shoulder angles, the EE pose follows from the human elbow position and orientation, with the end-effector orientated so that the upper arm always points to the center of the human shoulder. The end-effector's reference poses are computed coherently with the frequency of the NLP solution, meaning that a new pose is commanded to the robot every T_f/N seconds. A Cartesian impedance controller, running at 200 Hz, tracks the target end-effector poses. The stiffness and damping parameters of the controller were tuned experimentally.

However, commanding the Cartesian end-effector pose through (12) produces non-negligible tracking errors along the vertical axis. This issue is primarily due to the arm's weight, since early rehabilitation is typically administered with the human subject not yet able to support the weight of their own arm [44]. Impractically high stiffness levels, far exceeding what is safe for the subject, would be required to significantly improve the tracking. To remedy this, we implemented a gravity-compensation strategy that integrates the generalized torques u^* into the end-effector reference. More specifically, the vertical reference for the end-effector is adjusted by including the optimal value $u^{*,SE}$ of the vertical movements along the SE DoF, which account for arm weight and inertia through (3). This additional torque is transformed into the corresponding vertical force to be applied at the human elbow. Given the desired stiffness of the impedance controller along the vertical axis (K_z) , such a force can be realized at the end-effector by modulating the distance of the attractor from the current position:

$$^{\text{base}}\bar{p}_{\text{EE}}^{z} = ^{\text{base}}\hat{p}_{\text{EE}}^{z} + \frac{u^{*,\text{SE}}}{K_{z}L_{\text{hum}}\sin(\hat{\text{SE}})}$$
(13)

This compensation adjusts the robot's vertical reference, achieving the desired height set-point and fully supporting the human arm without high stiffness. The vertical force produced by the robot counteracts gravity on the arm at the desired elbow height, naturally descending from the personalized musculoskeletal model used in the trajectory optimization. Additionally, the formulation in (13) is robust to model inaccuracies: if the arm's actual weight differs from expectations, the impedance controller will stabilize at an equilibrium point. This is advantageous with respect to feedforward methods (i.e. [45]) that actively compensate for gravity, requiring accurate estimates of the subject's mass and its distribution.

F. Experimental setup and design

Our experimental setup included a KUKA LBR iiwa 7 robotic arm equipped with a custom-built brace that interfaces the human with the robot end-effector. The brace was shaped with a thermoplastic material to cradle the human elbow (see Fig. 3), and attached to the robot end-effector via screws. fixing the transformation between the robot EE frame and the human elbow frame. Through this elbow brace interface, the robot could impose a desired movement on the human and support the weight of their arm, while simultaneously estimating the human state. Computations were performed on a Dell Latitude 7420 laptop with an i7-1185G7 processor, interfaced with a dedicated Dell workstation with an Xeon W-2123 processor running the impedance controller. In this way, we ensured that the robot low-level controllers would receive commands at the required 200 Hz frequencies, regardless of potential delays in the high-level planning. ²

A healthy human subject acted as a patient in our labbased experiments. The brace interface was strapped onto the subject's arm, and they were instructed to maintain a constant pose for their torso with respect to the robot base. This satisfied the assumption of a stationary glenohumeral joint center employed in the model's state estimation. Our experimental protocol was approved by the TU Delft Human Research Ethics Committee (HREC).

To demonstrate the capabilities of our approach, we considered two scenarios: the early stages of the therapy, where the robot performs full guidance while the human subject is passively led through the movements, and the later stages of physical therapy, where the human subject gradually regains strength and actively participates in the movements. We describe each scenario in more detail below.

1) Passive human subject: when the subject passively follows the movement, their rotator cuff tendon strain is purely position-dependent. To guarantee low strains across all of the rotator cuff, tendon behavior was monitored through a strain map aggregating information regarding the maximum strain

 $^{^2\}mathrm{Prior}$ to paper acceptance, our software implementation is available by contacting the authors.

across all of the tendons. In other words, the strain value at a given model state \boldsymbol{x} represents the maximum strain observed across the supraspinatus, infraspinatus, subscapularis, and teres minor tendons. We locked the AR DoF so that the complete rehabilitation movement towards the target final state \boldsymbol{x}_d can be optimized and then executed in an open loop. We fixed the time horizon for the optimization to $T_f=5$ seconds and divided it into N=50 equal intervals. We determined the cost function weights for the real human-robot experiment via extensive simulations, to provide the potential user of our approach with general guidelines and understanding of parameter selection with respect to the desired behavior.

2) Active human subject: due to active human response during therapy, unforeseen modifications to the strain maps are to be taken into account. In particular, we are interested in how specific muscle activations can be accounted for in our pipeline. Without loss of generality, we present here therapy targeting the supraspinatus tendon specifically, selected as it is one of the most commonly injured within the rotator cuff [46]. As the supraspinatus muscle activation α_{ss} modifies tendon strain, our trajectory optimization must be reactive to adapt the optimal trajectory in real-time over the evolving strain map. As such, we considered a shorter planning horizon that allows us to compute and update the optimal trajectory in realtime ($T_f = 1$ second, N = 10 intervals), optimizing it over a receding horizon. First, we demonstrated in simulation the reactiveness of our trajectory optimization to different strain map variations, and then moved to closed-loop execution on the real robot. In this experiment, we left the AR DoF free, as our real-time replanning is able to handle generic variations to the 2D strain maps.

In a previous study, we demonstrated that surface electromyography (EMG) does not accurately reflect rotator cuff activity and strain [22]. Therefore, instead of using EMG to measure muscle activations, we emulated them and assessed their effect on tendon strain using OpenSim. During our experiments, the emulated activation was kept constant, presented sudden steps, or followed ramp profiles. These cases were considered as they cover conceptually both fast and slow variations in the activation of the subject's muscles during therapy. In the future, realistic activation estimates could be achieved with a real-time algorithm like our rapid muscle redundancy (RMR) solver [22]. Given the time-consuming setup and potential reliability issues of EMG, model-based or hybrid muscle activity estimation would be more practical for real physiotherapy applications.

III. RESULTS

A. Effect of OCP parameters on trajectories (passive subject)

We first ran BATON in simulation to examine the effects of optimization parameters and to determine the best relative cost function weights for synthesizing rehabilitation movements for passively assisted patients. We explored various permutations of the cost function weights $(w_{\sigma}, w_{\rm acc}, w_{\tau})$, with Fig. 4 showing some of the representative scenarios. We fixed $w_{\rm acc}=10$ to guarantee low accelerations on the human body and varied the other two parameters to achieve rather extreme cases. If

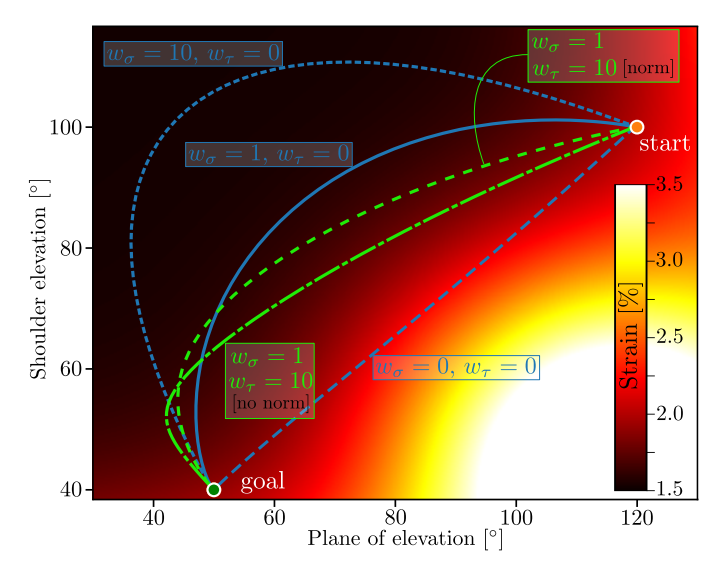


Fig. 4. Effect of tuning the cost function parameters on the optimal trajectories for the human DoF. In blue, the influence of w_{σ} on the optimal path. In green, the effect of normalizing L_{τ} when weighting the distance to the target final pose. To guarantee slow motions, we kept $w_{\rm acc}=10$.

no requirement of minimizing the strain is specified ($w_{\sigma}=0$), our optimization would drive the human arm towards the target goal pose along the shortest path (dashed blue line). When higher weights w_{σ} are used, the trajectory makes a wider excursion in the low-strain regions (solid and dotted blue lines). While this guarantees safer therapy, we observed that increasing this term gradually produces wider trajectories while the quantitative decrease in strain becomes negligible. In other words, wider excursions do minimize the cost function value, but they lead toinsignificant reductions in strain. Given this trade-off, we fixed $w_{\sigma}=1$ for later experiments.

With a passive subject, the strain map was fixed and did not vary with time. Thus, we could directly optimize the entire trajectory and execute it in an open-loop manner. In these conditions, the terminal condition in II-B2 is applied also to the final human pose, so the optimized trajectory reaches it even when $w_{\tau}=0$. This effectively simplifies the tuning of our cost function to only two parameters in this case. By selecting $w_{\rm acc}=10,\ w_{\sigma}=1$ the resulting trajectory traverses safe low-strain regions ($\sigma \leq 2\%$). These weights were used for the robot experiments in Sec. III-B below.

However, relying only on the terminal constraint to drive the human body to the target pose is not feasible when variations in the strain map can happen. Indeed, a trajectory that is safe on the initial map can end up crossing high-strain regions unexpectedly on the updated strain map. This motivates setting $w_{\tau} \neq 0$, and investigating the effect of normalizing the distance to the target L_{τ} on the optimal trajectory (Fig. 4, green lines). When L_{τ} was normalized by the initial distance from x_{τ} , lower-strain trajectories were produced, prioritizing strain minimization over approaching the goal earlier. This normalization ensured that the goal pose always provides a movement direction, while preventing the contribution to the cost function L from vanishing when the goal is closer or dominating when it is farther.

All the trajectories were simulated on the KUKA robot

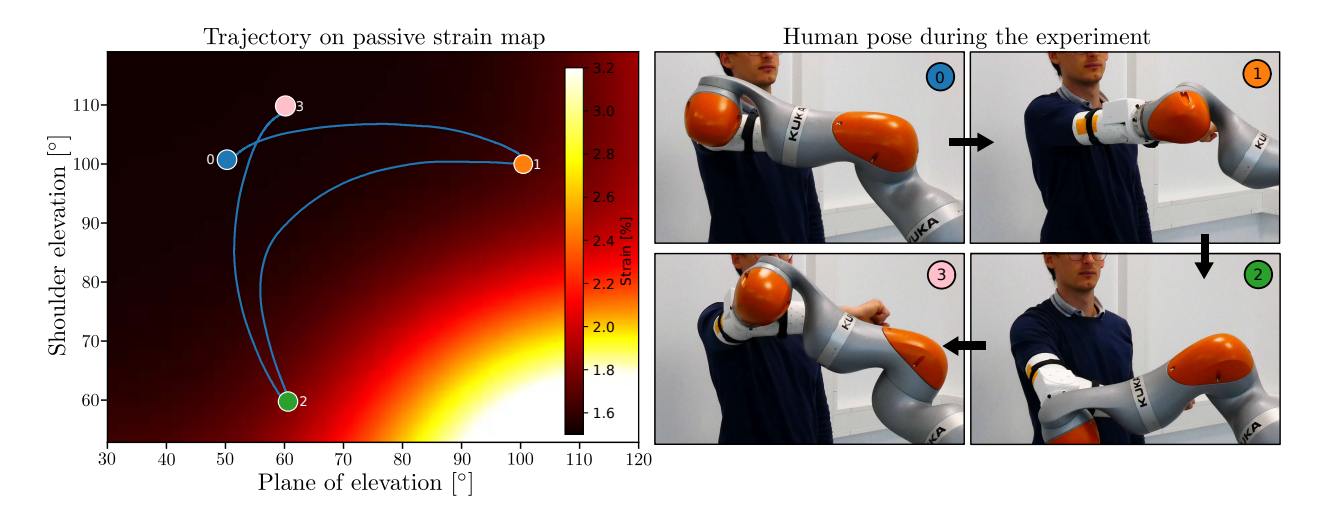


Fig. 5. Human trajectories produced for passive rehabilitation were visualized on the corresponding strain map (left). The blue line shows the actual trajectory, in human coordinates, along which the robot moved our subject. The paths connect target human poses given as goals to 3 instances of our trajectory optimization problem minimizing the maximum strain that the rotator cuff tendons encounter. The corresponding pose of the test subject is shown at the different target positions in the motion (right).

in Gazebo, to check for the robot's ability to reproduce the desired movements.

B. Quality of the executed paths (passive subject)

To demonstrate the performance of BATON in delivering therapy motion to a test subject by a real robot, we selected a few target poses around the shoulder state space to which the robot had to drive the subject. Figure 5 shows the experimental setup and the target poses on the strain map, together with the optimal trajectories that were delivered to our test subject by the robot. The robot started at the state marked by the blue dot in the low-strain zone. First, it moved the patient to the state marked by the orange dot and then toward the state indicated by the green dot to increase the level of strain and increase the range of motion. The resulting trajectory avoided higher strain regions and lower overall strain was achieved in the movement (Fig. 6, top row), permitting the exploration of a large range of motion with minimum risk of re-injury. Finally, the robot moved the shoulder state back into the low-strain zone denoted by the pink dot.

While human safety is more easily analyzed in the subject-centric coordinates on the strain map, the impedance controller tracks the desired optimal trajectory expressed in its base frame. The Cartesian reference positions for the robot endeffector are presented in Fig. 6 (last two rows), together with the actual end-effector poses across the duration of the experiment. In particular, the bottom row of the figure presents the tracking performance along the robot's vertical axis. As expected, the vertical reference z_{ref} is not reached, but the position mismatch $z_{ref}-z_{curr}$ allows the Cartesian impedance controller to provide the correct vertical force required to track the actual optimal end-effector height z_{opt} , which is obtained from our computed offset in (12).

C. Online adaptations (active subject)

1) Simulations: We investigated the responsiveness and adaptability of our control scheme when the strain maps

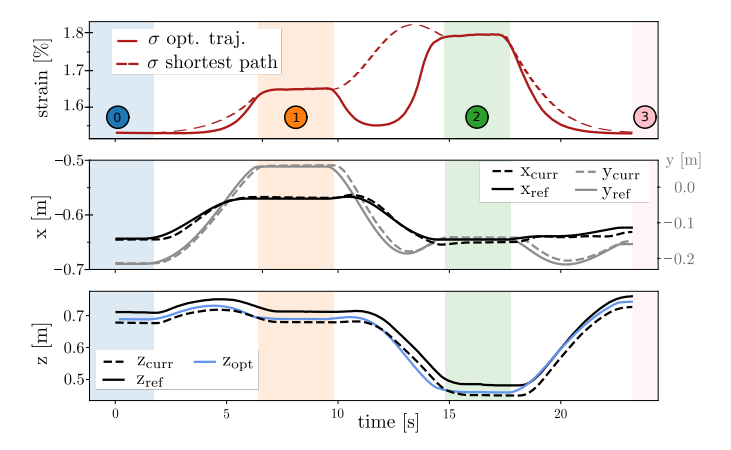


Fig. 6. Evolution of the strain level σ experienced by the human during passive therapy (above) and Cartesian coordinates of the robotic end-effector \mathbf{p}_{BE} during the experiment (below). The top graph compares σ during the experiment against the strain along the shortest paths between the beginning and end of each trajectory. The bottom graph highlights the effect of using the personalized musculoskeletal model to inform the gravity compensation of the human arm: the reference given to the controller (solid black) makes it so that the current position (dashed) tracks the real optimal one (solid blue).

change as a consequence of varying muscle activations. Muscle activation has a direct effect on the optimal path between two poses, since it affects the strain on the corresponding tendon, through (2). We studied this functionality in simulation to explore how various muscle activation patterns affect our rehabilitation trajectory, and to test our optimization with more drastic and challenging strain map variations. The initial model state was set at $SE_0 = PE_0 = 60^{\circ}$, while the target position to reach was set to $\overline{PE} = 45^{\circ}$, $\overline{SE} = 95^{\circ}$, requiring movement along multiple human DoFs. Owing to the shorter time horizon over which we ran our trajectory optimization, BATON was able to achieve a trajectory re-planning with an update rate of roughly 10 Hz. This permits us to generate new trajectories that can account for strain map variations, allowing us to control human movement in a closed-loop manner. We varied the (artificial) muscle activation level for the supraspinatus muscle to assess how the strain modifications

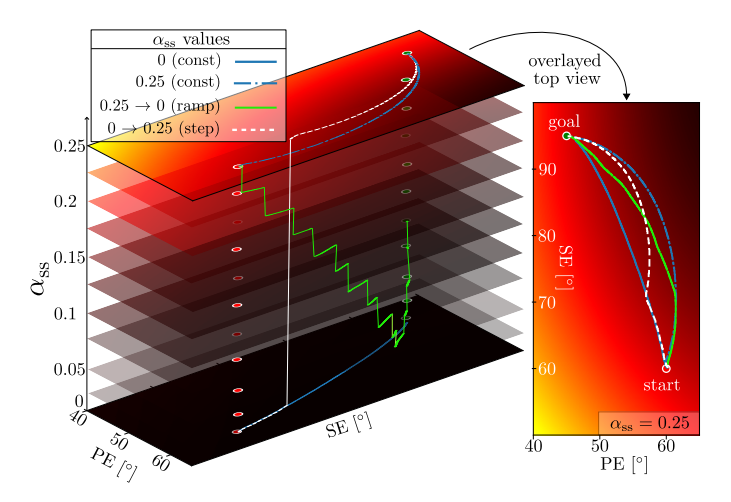


Fig. 7. The simulated effects of supraspinatus muscle activation (α_{ss}) on the optimal trajectory towards the same goal pose, when α_{ss} follows different activation profiles (green: decreasing ramp, white: step) or remains constant (blue). Large activation steps are used for ease of visualization, and all of the resulting trajectories are projected on the strain map corresponding to the highest α_{ss} for comparison to the right. Our musculoskeletal trajectory optimization is capable of accounting for sudden variations in the strain level, as a consequence, e.g., of varying muscle activation.

affect the resulting trajectories.

Fig. 7 demonstrates the effect of muscle activation variations: a sudden step increase in activation (white trajectory) and a gradual decrease in activation (green trajectory). These two cases are shown alongside the two boundary cases where activation is kept constantly high or low (resulting in the blue trajectories in the figure). On the right side of Fig. 7, we visualize all of the trajectories jointly on a single strain map, representing the strain landscape corresponding to the highest activation considered. Re-projecting all of the trajectories on the same plane allows one to see the different human trajectories produced by the gradual and sudden variations of the activation level, bounded by the two cases in which the activation was kept constant.

To understand the effects of more sudden and large changes in activation, for example, due to a strong reflex response, we tested cases in which BATON is presented with larger, more localized, and sudden variations in the strain maps. In this case, the initial and target human poses are inverted, representing the previous movement that evolved in the opposite direction (see Fig. 8). First, the strain map on which to plan has low strains, so the optimal trajectory points directly to the goal (Fig. 8, left). We then introduced a sudden large local variation in the landscape, so that higher strain appears along the direction of movement. BATON reacted to the variation by re-planing a new trajectory that keeps evolving towards the lower-strain region, deviating from the older plan proposed at the previous time step (white dots in the figure). Similarly, we introduced a second sudden large local variation in the strain map, observing a new trajectory adaptation that allows the simulated movement to remain safe.

2) Real system: having explored and compared the realtime adaptation of the reference optimal rehabilitation trajectories in simulation, we proceeded to demonstrate this in a real robotic-assisted experiment. The starting and the final human pose were the same as the first simulation experiment (respectively, $SE_0 = PE_0 = 60^{\circ}$, and $PE = 45^{\circ}$, $SE = 95^{\circ}$). As explained above, the muscle activation $\alpha_{\rm ss}$ was not directly measured by electromyography, but was emulated for the given task. The subject was guided through the same movement multiple times, during which the strain map varied to mimic interactive subject response due to time-dependent muscle activation. We demonstrate the real-time generation and tracking of the two extreme trajectories for $\alpha_{ss} = 0$ and $\alpha_{\rm ss}=0.25$ in Fig. 9, as simulation showed that the other cases would fall between these two. It can be noted that the algorithm can handle different levels of muscle activations by generating different rehabilitation movements, that are tracked in real-time by the Cartesian impedance controller. In particular, the two conditions lead to a difference of more than 10° along the plane-of-elevation axis. This difference was a result of adaptations to the human movements to traverse safer areas defined by the different muscle activity values.

D. Computational performance (active and passive subject)

We also used simulations to compare the computational efficiency of our choice to capture the human skeletal dynamics with OpenSimAD, against numerically querying the original OpenSim model during the optimization. This was done for an active subject as well as for a passive subject, modulating the time horizon for the trajectory optimization instances (4). In Tab. I, we report the average computation times for solving (4) when the system dynamics are enforced at the collocation points through the two different methods. The difference is roughly two orders of magnitude in favor of BATON, and real-time trajectory optimization was possible only with OpenSimAD, granting re-planning capabilities at a frequency of roughly 10 Hz with appropriate selection of the planning horizon and its discretization. BATON achieved the same computational performances during the robot experiments.

TABLE I COMPUTATION TIME TO SOLVE A SINGLE OCP INSTANCE WITH DIFFERENT TIME HORIZONS: A) PASSIVE SUBJECT, B) ACTIVE SUBJECT

Scenario	OpenSim+CasADi	OpenSimAD (BATON)
A $(T_f = 5 \text{ s}, N = 50)$	227.0 s	1.9 s
B $(T_f = 1 \text{ s}, N = 10)$	8.50 s	0.12 s

IV. DISCUSSION

We have developed a new approach to enable robot-based physiotherapy called BATON, which can automate and personalize rehabilitation through the navigation of underlying biomechanical outcomes. Achieving our first research aim, BATON directly couples human musculoskeletal outcomes to a robot controller through trajectory optimization. Embedding high-fidelity musculoskeletal outcomes is crucial for enabling the robotic system to deliver rehabilitation for rotator cuff injuries, where insights into patient biomechanics are paramount. Knowledge of the patient's range of motion and tissue loads is essential for optimizing safe movements that avoid high-strain configurations associated with high risks of re-injury. These biomechanical insights allowed us to plan and execute

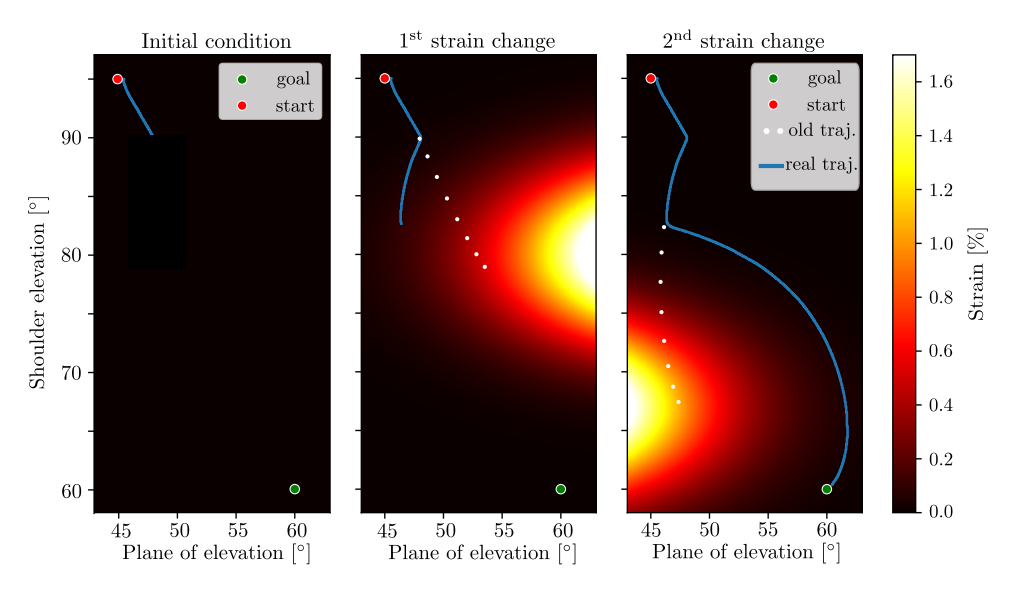


Fig. 8. Real-time trajectory optimization allows to account for sudden variations in the strain level. We show here how the optimal trajectory changes as a consequence of rapid variations in a (fabricated) strain map. The trajectory optimization starts on a strain map which is completely safe, generating a motion directly towards the goal (left). Sudden modifications to the strain cause the reference to avoid higher-strain zones (center and right), generating a trajectory that deviates from the shortest path adapting to the new scenarios, and prioritizing safety.

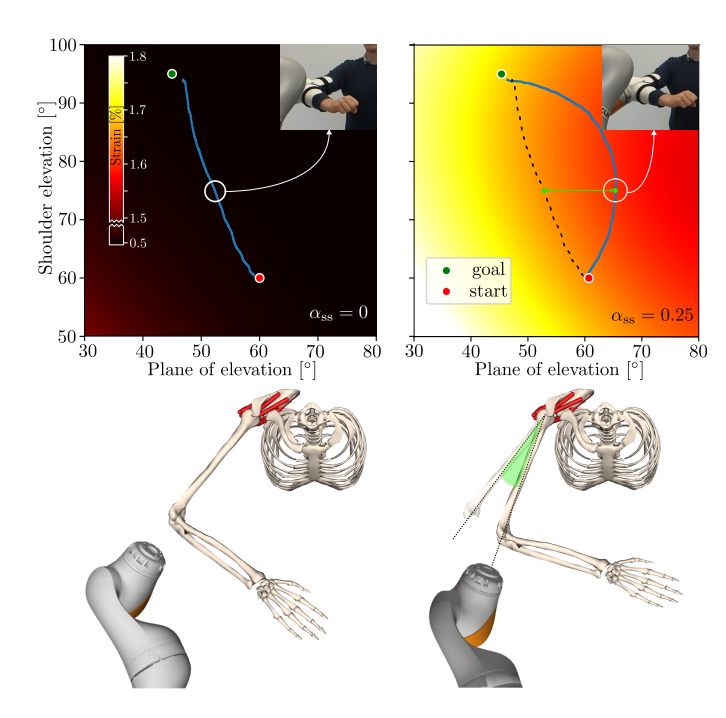


Fig. 9. Different supraspinatus activation α_{ss} causes different strain land-scapes for the corresponding tendon. Left: no activation - right: activation is increased, causing the lower-strain path to be different and leading the human through different shoulder poses. The same value of shoulder elevation is used to compare the two trajectories, showing a difference of more than 10° visualized both on the model and our human subject.

robotic rehabilitation trajectories, but can also be leveraged by experienced therapists to improve therapy's efficacy and safety.

To accomplish our second aim of real-time replanning capabilities, we decoupled the navigation of musculoskeletal loading into tissue loading landscapes as strain maps and algorithmically differentiable human dynamics for control. The tissue-loading landscape represents the navigable reha-

bilitation space, like a map of underwater reefs used to help a ship safely navigate, and the skeletal dynamics of the human shoulder describe the motion response of the vessel. This unique approach allows us to take advantage of the details of high-fidelity biomechanical models without facing prohibitive computational costs during real-time control. In both passive and active scenarios, we found BATON to operate several orders of magnitudes faster than using traditional musculoskeletal modeling and simulation techniques (Tab. I). As a result, real-time re-planning of reference trajectories for the rehabilitation robot was attained at an average update rate of just below 10 Hz. This allowed us to close the loop between sensing, optimization, and reference tracking both in simulation, where multiple edge-cases were investigated (Fig. 7 and Fig. 8), as well as on the real robot (Fig. 9). Besides improved computational efficiency, decoupling also provides a more modular overview of different aspects of the musculoskeletal system. For example, strain maps can provide an intuitive visual interpretation of strain mechanics as an indicator of re-injury risk during shoulder therapy.

Further, we analyzed the performances of BATON through simulations and physical experiments and achieved the third aim of this study. The optimized trajectories are tunable to achieve a trade-off between the minimization of tendon strain and the directness of the path (Fig. 4). We guaranteed a high-quality reproduction of the optimal path executed by the robot, including effective support of the subject's arm (Fig.5 and Fig.6). Through a combination of simulation and physical experiments, we demonstrated how BATON can quickly adapt to a changing strain landscape due to unforeseen changes in rotator cuff muscle activity.

Overall, our results demonstrate how embedding a highfidelity representation of the human musculoskeletal system in the controller improves physical human-robot interaction in the context of automated yet responsive rehabilitation. This unlocks the design of robotic controllers that can monitor musculoskeletal quantities that even experienced therapists lack access to, potentially enhancing the utility of these systems in clinical rehabilitation. The next step is to evaluate the system on target user and patient groups.

The different modalities (i.e., an active and a passive subject) explored in this study can provide solutions for different stages of the therapy. After surgery and in the initial phases of treatment after an injury, the patient is generally restricted in their mobility, and movements are carefully applied by the therapist who supports the arm and shoulder. We were able to control robot-applied movements over long-horizon trajectories to increase the range of motion of the shoulder while minimizing tendon strain in the rotator cuff to avoid re-injury (Fig. 5). As treatment progresses and as the patient regains strength and mobility, patients become and are encouraged to be more active during the exercises, in which case navigation must be more responsive. We tested rapid changes in muscle activation simulating patient reactions, to show that high-strain regions (even due to emerging activation) are successfully avoided using the active real-time re-planning of our biomechanics-aware trajectory optimization methods.

While this study demonstrated and evaluated key aspects of the novel method, we acknowledge that there are some limitations that require interesting future work. We described the state of the human shoulder focusing on the mobility of the glenohumeral joint alone, and planned human motions along two DoFs (PE and SE). In our setting, the motion along the third DoF (AR) of the human glenohumeral joint was not optimized, and the current value of AR determined the strain map on which the optimization took place. This simplification allowed us to validate the core concept, but spatial (3D) rehabilitation trajectories should be investigated for real-world applications. For example, while the strain of the rotator cuff tendon depends on the relative position between the upper arm and the shoulder blade, other movement DoFs, such as the scapula mobility or the human torso orientation, can also influence tissue loading in the shoulder. The human pose estimation that we employed did not include other DoFs and may rely on simplifying assumptions that are too restrictive for a wide range of physical therapy applications. While an accurate estimation of the subject's body motion was beyond the scope of this work, better methods to monitor human posture and movement could be integrated. Viable options could rely on motion capture techniques, which offer high precision but are difficult to deploy, while video camera systems or IMUs might be more practical but also less reliable. Apart from resulting in more complex computations, a challenging aspect of treating additional DoFs is delivering visual information that a patient/therapist can easily interpret. In the future, we will explore how to extend BATON to also include additional DoFs, such as those related to the scapula, with an approach to measure the state of the scapula itself.

Another limitation is related to estimating realistic muscle activations. We simulated muscle activations to test extreme conditions for BATON and verify that the planned trajectories remained in low-strain regions to give us confidence that the automated responses are safe. Additionally, using simulated

activations ensured the repeatability and reproducibility of the responses. As such, while these activations may not be physiological, including these extremes allowed us to test the worstcase scenario of abrupt human responses and show BATON's potential to be safe under these conditions. It is important to note that the rotator cuff muscles are not accessible by common surface electromyography, and direct measurement would be impossible during physiotherapy. In the future, we plan to integrate our novel rapid model-based techniques (e.g., RMR solver [22]) into BATON so that muscle activities can be estimated reliably. Since the RMR solver requires only human pose and interaction forces as input, it is a very promising candidate for estimating physiologically plausible muscle forces and activations. The formulation of the RMR solver would enable us to retain real-time capabilities and to account for activation dynamics as well. When considering real muscle activations, resorting to predictive methods like BATON for synthesizing safe physical human-robot interaction will be even more important, allowing a robot to plan movements to minimize other relevant physical quantities such as interaction forces between the human and the robot, and joint reaction forces.

V. CONCLUSION

We have presented a novel approach to physical humanrobot interaction that leverages biomechanical-aware trajectory optimization to generate and execute rehabilitation trajectories applied by a real robot to a human subject, leveraging a personalized musculoskeletal model. We demonstrated BATON for planning robot-assisted movements that account for the mechanical strain in the rotator cuff tendons, both during the early stages of rehabilitation when the human is passively guided, and as muscle activation emerges when the subject actively responds during in therapy. In contrast to previous robotic approaches where computationally expensive biomechanical metrics were not considered, we took the first step in unlocking the use of high-fidelity musculoskeletal models in real-time biomechanics-aware robotic controllers. While our work focuses on physiotherapy robotics, the ability of automated systems to estimate and respond to the changing internal states of the human body can resonate far beyond physical therapy. Our approach can enable the development of the next generation of biomechanical-aware controllers, and pass the "baton" to researchers in related fields of ergonomics, exoskeleton control, movement disorders, etc., where automatic, responsive, and personalized robotics can transform outcomes.

REFERENCES

- [1] H. Minagawa, N. Yamamoto, H. Abe, M. Fukuda, N. Seki, K. Kikuchi, H. Kijima, and E. Itoi, "Prevalence of symptomatic and asymptomatic rotator cuff tears in the general population: from mass-screening in one village," *Journal of orthopaedics*, vol. 10, no. 1, pp. 8–12, 2013.
- [2] A. Leclerc, J. Chastang, I. Niedhammer, M. Landre, and Y. Roquelaure, "Incidence of shoulder pain in repetitive work," *Occupational and environmental medicine*, vol. 61, no. 1, pp. 39–44, 2004.
- [3] S. T. Seroyer, S. J. Nho, B. R. Bach Îr, C. A. Bush-Joseph, G. P. Nicholson, and A. A. Romeo, "Shoulder pain in the overhead throwing athlete," *Sports health*, vol. 1, no. 2, pp. 108–120, 2009.

- [4] S. Thomson, C. Jukes, and J. Lewis, "Rehabilitation following surgical repair of the rotator cuff: a systematic review," *Physiotherapy*, vol. 102, no. 1, pp. 20–28, 2016.
- [5] M. Sommerhalder, Y. Zimmermann, J. Song, R. Riener, and P. Wolf, "Polymorphic control framework for automated and individualized robot-assisted rehabilitation," *IEEE Transactions on Robotics*, 2023.
- [6] L. Marchal-Crespo and D. J. Reinkensmeyer, "Review of control strategies for robotic movement training after neurologic injury," *Journal of neuroengineering and rehabilitation*, vol. 6, pp. 1–15, 2009.
- [7] D. Calafiore, F. Negrini, N. Tottoli, F. Ferraro, O. Ozyemisci-Taskiran et al., "Efficacy of robotic exoskeleton for gait rehabilitation in patients with subacute stroke: a systematic review," European Journal of Physical and Rehabilitation Medicine, vol. 58, no. 1, p. 1, 2022.
- [8] K. Y. Nam, H. J. Kim, B. S. Kwon, J.-W. Park, H. J. Lee, and A. Yoo, "Robot-assisted gait training (lokomat) improves walking function and activity in people with spinal cord injury: a systematic review," *Journal* of neuroengineering and rehabilitation, vol. 14, pp. 1–13, 2017.
- [9] P. K. Jamwal, S. Hussain, and M. H. Ghayesh, "Robotic orthoses for gait rehabilitation: An overview of mechanical design and control strategies," *Proceedings of the Institution of Mechanical Engineers, Part H: Journal* of Engineering in Medicine, vol. 234, no. 5, pp. 444–457, 2020.
- [10] K. L. Poggensee and S. H. Collins, "How adaptation, training, and customization contribute to benefits from exoskeleton assistance," *Science Robotics*, vol. 6, no. 58, p. eabf1078, 2021.
- [11] Y. Cen, J. Yuan, S. Ma, J. Luo, and H. Wang, "Trajectory optimization algorithm of trajectory rehabilitation training mode for rehabilitation robot," in 2022 IEEE International Conference on Robotics and Biomimetics (ROBIO). IEEE, 2022, pp. 2153–2158.
- [12] B. Luciani, L. Roveda, F. Braghin, A. Pedrocchi, and M. Gandolla, "Trajectory learning by therapists' demonstrations for an upper limb rehabilitation exoskeleton," *IEEE Robotics and Automation Letters*, 2023.
- [13] C. Fang, L. Peternel, A. Seth, M. Sartori, K. Mombaur, and E. Yoshida, "Human modeling in physical human-robot interaction: A brief survey," *IEEE Robotics and Automation Letters*, 2023.
- [14] M. G. Carmichael and D. Liu, "Estimating physical assistance need using a musculoskeletal model," *IEEE Transactions on Biomedical Engineering*, vol. 60, no. 7, pp. 1912–1919, 2013.
- [15] B. Ghannadi, N. Mehrabi, R. S. Razavian, and J. McPhee, "Nonlinear model predictive control of an upper extremity rehabilitation robot using a two-dimensional human-robot interaction model," in 2017 IEEE/RSJ International Conference on Intelligent Robots and Systems (IROS). IEEE, 2017, pp. 502–507.
- [16] A. Zignoli, F. Biral, K. Yokoyama, and T. Shimono, "Including a musculoskeletal model in the control loop of an assistive robot for the design of optimal target forces," in *IECON 2019-45th Annual Conference of the IEEE Industrial Electronics Society*, vol. 1. IEEE, 2019, pp. 5394–5400.
- [17] J. Fang and Y. Yuan, "Human-in-the-loop optimization of wearable robots to reduce the human metabolic energy cost in physical movements," *Robotics and Autonomous Systems*, vol. 127, p. 103495, 2020.
- [18] D. F. Gordon, C. McGreavy, A. Christou, and S. Vijayakumar, "Humanin-the-loop optimization of exoskeleton assistance via online simulation of metabolic cost," *IEEE Transactions on Robotics*, vol. 38, no. 3, pp. 1410–1429, 2022.
- [19] K. Li, M. Tucker, R. Gehlhar, Y. Yue, and A. D. Ames, "Natural multicontact walking for robotic assistive devices via musculoskeletal models and hybrid zero dynamics," *IEEE Robotics and Automation Letters*, vol. 7, no. 2, pp. 4283–4290, 2022.
- [20] D. G. Thelen, F. C. Anderson, and S. L. Delp, "Generating dynamic simulations of movement using computed muscle control," *Journal of biomechanics*, vol. 36, no. 3, pp. 321–328, 2003.
- [21] F. De Groote and A. Falisse, "Perspective on musculoskeletal modelling and predictive simulations of human movement to assess the neuromechanics of gait," *Proceedings of the Royal Society B*, vol. 288, no. 1946, p. 20202432, 2021.
- [22] I. Belli, S. Joshi, J. M. Prendergast, I. Beck, C. Della Santina, L. Peternel, and A. Seth, "Does enforcing glenohumeral joint stability matter? a new rapid muscle redundancy solver highlights the importance of non-superficial shoulder muscles," *Plos one*, vol. 18, no. 11, p. e0295003, 2023.
- [23] A. Falisse, G. Serrancolí, C. L. Dembia, J. Gillis, I. Jonkers, and F. De Groote, "Rapid predictive simulations with complex musculoskeletal models suggest that diverse healthy and pathological human gaits can emerge from similar control strategies," *Journal of The Royal Society Interface*, vol. 16, no. 157, p. 20190402, 2019.

- [24] C. L. Dembia, N. A. Bianco, A. Falisse, J. L. Hicks, and S. L. Delp, "Opensim moco: Musculoskeletal optimal control," *PLOS Computational Biology*, vol. 16, no. 12, p. e1008493, 2020.
- [25] E. Peiros, Z.-Y. Chiu, Y. Zhi, N. Shinde, and M. C. Yip, "Finding biomechanically safe trajectories for robot manipulation of the human body in a search and rescue scenario," in 2023 IEEE/RSJ International Conference on Intelligent Robots and Systems (IROS). IEEE, 2023, pp. 167–173.
- [26] V. Vatsal and G. Hoffman, "Biomechanical motion planning for a wearable robotic forearm," *IEEE Robotics and Automation Letters*, vol. 6, no. 3, pp. 5024–5031, 2021.
- [27] C. Latella, Y. Tirupachuri, L. Tagliapietra, L. Rapetti, B. Schirrmeister, J. Bornmann, D. Gorjan, J. Čamernik, P. Maurice, L. Fritzsche et al., "Analysis of human whole-body joint torques during overhead work with a passive exoskeleton," *IEEE Transactions on Human-Machine Systems*, vol. 52, no. 5, pp. 1060–1068, 2021.
- [28] X. Bao, Z. Sheng, B. E. Dicianno, and N. Sharma, "A tube-based model predictive control method to regulate a knee joint with functional electrical stimulation and electric motor assist," *IEEE Transactions on Control Systems Technology*, vol. 29, no. 5, pp. 2180–2191, 2020.
- [29] G. Clark and H. B. Amor, "Learning ergonomic control in human–robot symbiotic walking," *IEEE Transactions on Robotics*, vol. 39, no. 1, pp. 327–342, 2022.
- [30] J. M. Prendergast, S. Balvert, T. Driessen, A. Seth, and L. Peternel, "Biomechanics aware collaborative robot system for delivery of safe physical therapy in shoulder rehabilitation," *IEEE Robotics and Automa*tion Letters, vol. 6, no. 4, pp. 7177–7184, 2021.
- [31] S. Balvert, J. M. Prendergast, I. Belli, A. Seth, and L. Peternel, "Enabling patient-and teleoperator-led robotic physiotherapy via strain map segmentation and shared-authority," in 2022 IEEE-RAS 21st International Conference on Humanoid Robots (Humanoids). IEEE, 2022, pp. 246– 253.
- [32] P. K. Jamwal, S. Hussain, Y. H. Tsoi, and S. Q. Xie, "Musculoskeletal model for path generation and modification of an ankle rehabilitation robot," *IEEE Transactions on Human-Machine Systems*, vol. 50, no. 5, pp. 373–383, 2020.
- [33] A. Seth, M. Dong, R. Matias, and S. Delp, "Muscle contributions to upper-extremity movement and work from a musculoskeletal model of the human shoulder," *Frontiers in neurorobotics*, vol. 13, p. 90, 2019.
- [34] S. L. Delp, F. C. Anderson, A. S. Arnold, P. Loan, A. Habib, C. T. John, E. Guendelman, and D. G. Thelen, "Opensim: open-source soft-ware to create and analyze dynamic simulations of movement," *IEEE transactions on biomedical engineering*, vol. 54, no. 11, pp. 1940–1950, 2007.
- [35] A. Seth, J. L. Hicks, T. K. Uchida, A. Habib, C. L. Dembia, J. J. Dunne, C. F. Ong, M. S. DeMers, A. Rajagopal, M. Millard et al., "Opensim: Simulating musculoskeletal dynamics and neuromuscular control to study human and animal movement," PLoS computational biology, vol. 14, no. 7, p. e1006223, 2018.
- [36] Y. Chen, F. Jiang, H. Li, S. Chen, Y. Qiao, Y. Li, Y. Hua, J. Chen, and Y. Ge, "Retears and concomitant functional impairments after rotator cuff repair: shoulder activity as a risk factor," *The American Journal of Sports Medicine*, vol. 48, no. 4, pp. 931–938, 2020.
- [37] R. Drillis, R. Contini, and M. Bluestein, "Body segment parameters," Artificial limbs, vol. 8, no. 1, pp. 44–66, 1964.
- [38] I. Beck, I. Belli, L. Peternel, A. Seth, and J. M. Prendergast, "Real-time tendon strain estimation of rotator-cuff muscles during robotic-assisted rehabilitation," in 2023 IEEE-RAS 22nd International Conference on Humanoid Robots (Humanoids). IEEE, 2023, pp. 1–8.
- [39] A. Falisse, G. Serrancolí, C. L. Dembia, J. Gillis, and F. De Groote, "Algorithmic differentiation improves the computational efficiency of opensim-based trajectory optimization of human movement," *PLoS One*, vol. 14, no. 10, p. e0217730, 2019.
- [40] J. A. E. Andersson, J. Gillis, G. Horn, J. B. Rawlings, and M. Diehl, "CasADi – A software framework for nonlinear optimization and optimal control," *Mathematical Programming Computation*, vol. 11, no. 1, pp. 1–36, 2019.
- [41] D. Garg, M. Patterson, W. Hager, A. Rao, D. R. Benson, and G. T. Huntington, "An overview of three pseudospectral methods for the numerical solution of optimal control problems," *hal-01615132*, 2017.
- [42] A. Wächter and L. T. Biegler, "On the implementation of an interiorpoint filter line-search algorithm for large-scale nonlinear programming," *Mathematical programming*, vol. 106, pp. 25–57, 2006.
- [43] I. S. Duff and J. K. Reid, "The multifrontal solution of indefinite sparse symmetric linear," ACM Transactions on Mathematical Software (TOMS), vol. 9, no. 3, pp. 302–325, 1983.

- [44] P. C. Lastayo, T. Wright, R. Jaffe, and J. Hartzel, "Continuous passive motion after repair of the rotator cuff. a prospective outcome study," *JBJS*, vol. 80, no. 7, pp. 1002–11, 1998.
- [45] M. Manzano, S. Guégan, R. Le Breton, L. Devigne, and M. Babel, "Model-based upper-limb gravity compensation strategies for active dynamic arm supports," in 2023 International Conference on Rehabilitation Robotics (ICORR). IEEE, 2023, pp. 1–6.
- [46] J. Zhao, M. Luo, G. Liang, M. Wu, J. Pan, L.-f. Zeng, W. Yang, and J. Liu, "Risk factors for supraspinatus tears: a meta-analysis of observational studies," *Orthopaedic Journal of Sports Medicine*, vol. 9, no. 10, p. 23259671211042826, 2021.